PHYSICAL REVIEW A **90**, 021801(R) (2014)

Long-lived waveguides and sound-wave generation by laser filamentation

Oren Lahav,* Liad Levi, Itai Orr, Ron A. Nemirovsky, Jonathan Nemirovsky, Ido Kaminer, Mordechai Segev, and Oren Cohen*
Solid State Institute and Physics Department, Technion, Haifa 32000, Israel
(Received 8 August 2013; revised manuscript received 16 June 2014; published 19 August 2014)

We discover long-lived (microsecond-scale) optical waveguiding in the wake of atmospheric laser filaments. We also observe the formation and then outward propagation of the consequent sound wave. These effects may be used for remote induction of atmospheric long-lived optical structures from afar which could serve for a variety of applications.

DOI: 10.1103/PhysRevA.90.021801 PACS number(s): 42.65.Re, 42.82.Et, 52.38.Hb

The propagation of self-guided laser filaments through air and other gases results in a rich variety of phenomena and applications [1–3]. A laser filament is formed when a femtosecond pulse, with a peak intensity above the critical power for collapse (3 GW in air at an optical wavelength of 800 nm), is propagating in the otherwise transparent medium [1]. In air, the diameter of a filament is approximately 100 μm and it can propagate over distances much longer than the Rayleigh length, from several cm up to the kilometer range [4–7]. A filament is formed due to a dynamic balance between the linear diffractive and dispersive properties of the medium and its nonlinear features such as the self-focusing optical Kerr effect and defocusing due to the free electrons which are released from molecules through multiphoton ionization. In the atmosphere, filaments can be initiated at predefined remote distances [4,5] and propagate through fog, clouds, and turbulence [8,9]. Thus, filaments are attractive for atmospheric applications such as remote spectroscopy [8,10] and laser-induced water condensation [11].

An atmospheric filament pulse initiates complex nonlinear dynamics in the densities of free electrons and ions, air density, and in the level of molecular alignment. However, all of these effects are generally believed to die out after $<$10 ns. Experimental data about the long-term dynamics is especially scarce. The filamenting pulse leaves behind free electrons at initial densities of 10^{16}–10^{17} cm^{-3} [2,3], mostly from multiphoton ionization of oxygen molecules (because the ionization potential of N_2 molecules is significantly larger: 12 and 16 eV for O_2 and N_2, respectively). Initially, the free-electron density exhibits a radial bell-shaped profile. It is now established that 100 ps to $\sim$1 ns later, a shock wave of electron density forms and propagates outward supersonically [12–15]. The resultant radially increasing plasma density can be used for guiding a delayed laser pulse [12–15] or a microwave pulse [16]. However, recombination between the free electrons and positive oxygen molecules decreases the plasma density by two orders of magnitude and limits this waveguiding effect to a few nanoseconds. Such nanosecond dynamics of charge carriers also results in the emission of a high power burst of terahertz radiation [17]. Subsequently, when the density of free electrons decreases to below 10^{14} cm^{-3}, the capture of free electrons by neutral oxygen molecules (with a characteristic time of 150 ns), becomes dominant [18]. The influence of this oxygen ion population on the refractive index needs to be explored, thus it is yet unknown if it can contribute to waveguiding or antiguiding effects. Another effect induced by the filamentation is impulsive rotational excitation in the N_2 and O_2 molecules [19], where the molecules exhibit periodic revivals of molecular alignment for several tens of picoseconds after the passing of the filamenting pulse. Consequently, the refractive index of the air undergoes anisotropic temporal modulation [20]. This mechanism was used for guiding properly delayed picosecond pulses [21,22], but at times larger than several nanoseconds after the filamenting pulse, even this process does not leave behind any waveguiding effects. *In fact, processes resulting from plasma or molecular alignment in the wake of atmospheric laser filaments are limited to the first few nanoseconds.* Consequently, it was generally believed that 10 ns after the filamenting pulse, the medium does not exhibit any optical effect. In contrast to that, it was recently discovered that, 0.1–1 ms after the filament, there is a circular negative index change due to reduced air density that acts as an antiguide by defocusing a probe beam [23]. Altogether, thus far, experiments and theories on laser filamentation in the atmosphere concluded that there is no long-lived ($>$10 ns) waveguiding effect left behind the femtosecond filamenting pulse. This severely limits any cw application of laser filamentation, because the repetition rate of any high power laser used for creating the filament is low, hence for most of the time between pulses light would not be guided. Likewise, any other potential application would have to "live" on a picosecond to nanosecond scale, because at later times, waveguiding by the filament was thought to be nonexistent.

Here, we show the exact opposite: We demonstrate that the filament induces a transient refractive index change structure, on a microsecond scale, that enables optical waveguiding. This guiding is facilitated by the consequent acoustic wave which is generated by the filament. We show, through numerical simulations, that the dynamics of the air density, which results from the sudden heating, forms an annular region of increased air density. This ring-shaped positive refractive index pattern appears to have several guided modes. We demonstrate waveguiding through this induced annular refractive index structure. In addition, we observe and study the formation of ultrashort acoustic waves and subsequently their outward propagation at the speed of sound. Such induced long-lived waveguides can be useful for numerous applications of laser filamentation in the atmosphere, from power transmission through these channels to backward propagation of coherent and incoherent radiation for remote sensing.

*Corresponding authors: orenla@tx.technion.ac.il; oren@technion.ac.il

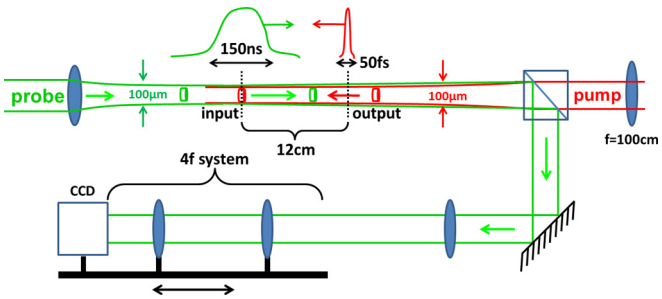

FIG. 1. (Color online) Scheme of the experimental setup. A Ti:sapphire pulsed laser 1-cm-wide beam with 50 fs time duration, central wavelength of 800 nm, 1 mJ per pulse at 1 kHz repetition rate, is focused into a diameter of ∼100 μm, creating a filament of ∼12 cm in the free air. The probe beam is a weak 527-nm pulsed laser beam, with a duration time of 150 ns and repetition rate of 1 kHz, triggered by the femtosecond laser. The delay between the pulses is controlled electronically and can span a range of 1 ms. In the filament region, the probe and pump beams propagate in opposite directions. The "input" and "output" planes correspond to the *probe* pulse entrance and exit planes of the filament channel, respectively. An imaging system images the probe pulse at the input and output planes. In the experiment presented in Fig. 4, we insert a lens that focuses the probe beam to a diameter of ∼100 μm at the input plane. No focusing lens is used in the experiments presented in Figs. 2 and 3, hence the probe beam is approximately a plane wave.

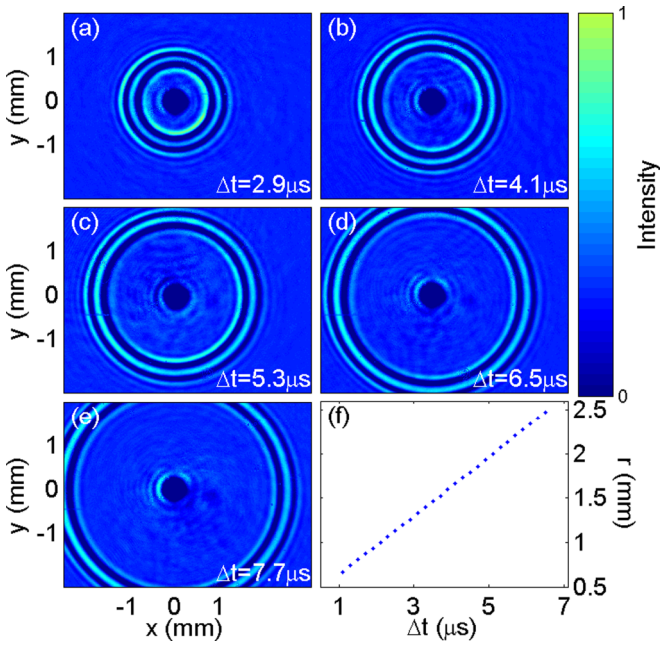

FIG. 2. (Color online) Outward propagation of the acoustic pulse. Shown are the intensity structures of the probe beam (plane wave) at the output plane for delay times of Δt = (a) 2.9, (b) 4.1, (c) 5.3, (d) 6.5, and (e) 7.7 μs after the filamenting pulse. Here, $\Delta t = 0$ corresponds to the time delay for which the probe and pump pulses collide within the filament channel. (f) Radius of the leading crest vs delay time. The calculated angle of the line corresponds to a velocity of 333 ± 1 m/s.

Our experimental methodology relies on using an electronically delayed short optical pulse for probing the long-term effects generated by a femtosecond filamenting pulse in the atmosphere. The experimental setup is shown in Fig. 1. A "pump" Ti:sapphire (wavelength centered around 0.8 μm) pulsed laser beam 1 cm wide with a 50 fs time duration, 1 mJ energy/pulse, and at 1 kHz repetition rate is focused to a diameter of ∼100 μm using an $f = 100$ cm lens. The expected Rayleigh range of such a beam is of the order of 2 cm. Our beam forms a filament of ∼12 cm length in the free air. We probe the filament wake using a weak pulsed laser beam of wavelength 527 nm, with a 150 ns pulse duration and 1 kHz repetition rate, which is triggered by the femtosecond laser. The delay between the probe pulse and the pump pulse is controlled electronically and can span a range of 1 ms. The pump and probe beams propagate in opposite directions. This setting helps in unraveling the induced index change, as the phase change accumulates along the filament, and at the same time the counterpropagation geometry makes it easy to separate the probe beam from the pump beam. We define the "input" and "output" planes as the entrance and exit planes of the *probe* pulse, which is propagating within the channel induced by the filament. A lens, a movable $4f$ system, and a CCD camera are used to image the probe beam at the input and output planes.

We first present the optical observation of the outward-propagating radial sound-wave pulse, produced in the wake of the filament. This sound wave has so far been explored experimentally by acoustic probing [24]. In this experiment we expand the probe beam such that it is approximately a plane wave at the input. Figures 2(a)–2(e) show the intensity of the output probe beam for several delay times with respect to the filament pulse (where $\Delta t = 0$ corresponds to time delay at which the centers of the probe and pump pulses coincide in the filament region). The acoustic wave is clearly revealed because it consists of regions with high and low air density that, respectively, exhibit positive and negative index changes. Figure 2(f) shows the radius of the leading crest versus delay time, from which we calculate the wave velocity to be 333 ± 1 m/s. This value is comparable to the sound velocity in air, thereby showing that the wave is indeed an acoustic wave. After the radial acoustic wave is emitted, a negative index change is left behind at the center. This negative index change, which decays slowly and is still observed even after 1 ms, was explored in Ref. [23]. However, the temporal resolution (∼40 μs) in the experiment of Ref. [23] was set by an electronic shutter that controlled the input light to the CCD. As such, that experiment was insensitive to the dynamics during the first several microseconds after the passing of the filamenting pulse. For this reason, the experiments in Ref. [23] could not reveal the waveguiding effect that is presented below. We now focus on early delay times, when the acoustic wave is formed, and propagate within the filament region. Figures 3(a)–3(i) show the intensity of the output probe beam for several delay times in the range between −40 ns and 1.4 μs. It is clearly shown that light is attracted towards the filament region by the forming acoustic wave. We find that this attraction of the light towards the filament region is robust to wind (we tested it with a blower of compressed air) and it occurs over a broad range of experimental parameters, such as different pulse energies and repetition rates.

Figure 3 suggests that the filaments induce a transient long-lived (microsecond-scale) annular waveguide. In order to

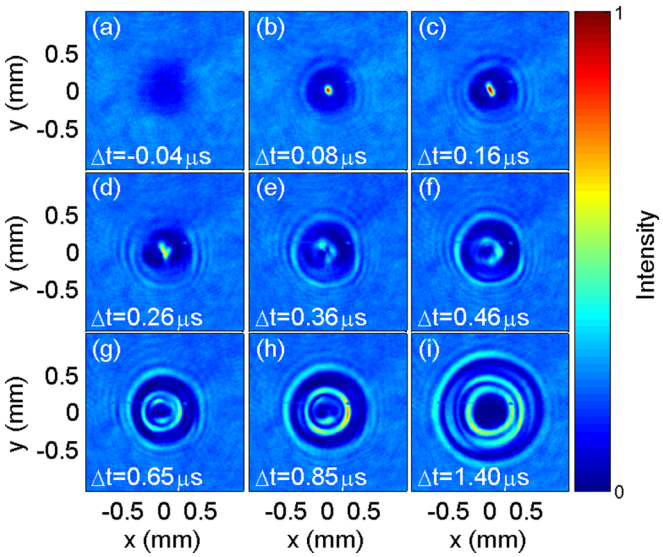

FIG. 3. (Color online) Long-lived index change in the filament wake. Shown are the intensity patterns of the probe beam at the output plane, for delay times of Δt = (a) −0.04, (b) 0.08, (c) 0.16, (d) 0.26, (e) 0.36, (f) 0.46, (g) 0.65, (h) 0.85, and (i) 1.4 μs after the filamenting pulse.

understand the origins of this filament-induced waveguiding phenomenon, we insert an $f = 100$ cm lens that focuses the probe beam into a diameter of ∼100 μm at the input plane [Fig. 4(a)], and explore its propagation at various delay

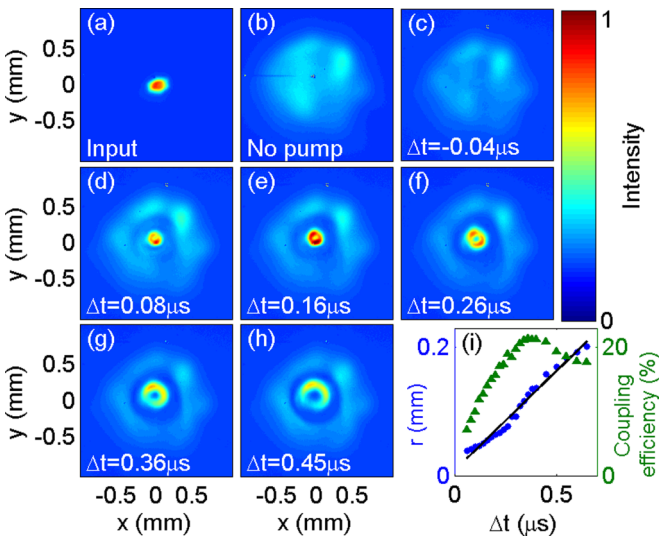

FIG. 4. (Color online) Long-lived filament-induced ring-shaped waveguide. (a) Intensity structure of the focused probe beam at the input plane. (b) Intensity structure of the probe beam at the output plane when the pump beam is blocked, i.e., no filament is formed. In the absence of the filament, the probe beam exhibits considerable diffraction broadening. (c)–(h) Intensity structures of the guided probe beam at the output plane for delay times of Δt = (c) −0.04, (d) 0.08, (e) 0.16, (f) 0.26, (g) 0.36, and (h) 0.45 μs with respect to the filamenting pulse. (i) Radius of the acoustic wave (blue dots) and coupling efficiency (green triangles) as a function of time delay. The black line is a linear fit of the radius with slope corresponding to a velocity of 310 ± 9 m/s.

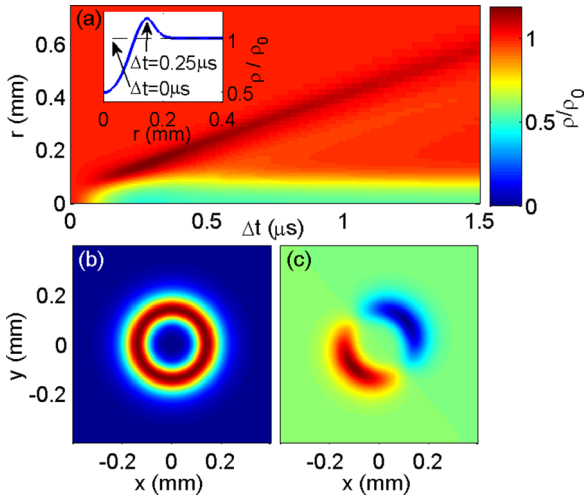

FIG. 5. (Color online) Numerical simulations of the filament wake. (a) Radial air density [$\rho(r)$] as a function of time delay. At the beginning ($\Delta t = 0$) the medium is homogeneous, i.e., $\rho(r) = \rho_0$. The density at the center ($r = 0$) initially becomes lower due to the sudden heating. The air moves outward radially, creating an acoustic wave with higher density. Regions with higher air density exhibit a positive refractive index change which forms a waveguide. Inset: Density profiles at time delays of $\Delta t = 0$ μs (dashed line) and $\Delta t = 0.25$ μs (solid line) after the filamenting pulse. (b), (c) The first two guided modes of the refractive index structure formed in the wake of the filament.

times. When the pump beam is blocked, hence no filament is present, the probe beam is propagating in free air and is broadening due to linear diffraction to a 1.2-mm [full width at half maximum (FWHM)] beam [Fig. 4(b)]. In this case, only 4% of the output power is still confined within the filament region. In contrast, after a filament has formed, the probe beam is guided within the ring-shaped positive index change resulting from the acoustic wave. Figures 4(c)–4(h) show the intensity of the probe beam at the output plane for several time delays, after the pump pulse has created the 12-cm-long filament. *Clearly, the probe beam is indeed guided within the waveguide induced by the filament.* The coupling efficiency into the induced waveguide region, as a function of time delay, is shown in Fig. 4(i). For example, the fraction of optical power contained within the filament region after 360 ns is 21% (i.e., more than 5 times larger than the linear propagation case). This experiment unequivocally shows that the filament induces a long-lived waveguide in the wake of the filament.

Finally, we investigate the formation of the annular waveguide numerically. We simulate the dynamics of the air density using hydrodynamic simulations, following the model presented in Ref. [23]. The simulated dynamics is depicted in Fig. 5(a). As shown there, shortly after the pump pulse has initiated the filamentation process, the air expands outward from the beam axis. This happens because the pump beam heats the gas and therefore creates a local peak in the air pressure. As a result of the rapid expansion, an acoustic wave is formed, surrounding the filament region with increased air density [Fig. 5(a) and the inset therein]. The higher density implies a higher refractive index, thus the ring-shaped structure

is essentially a ring-shaped waveguide. Solving numerically for the eigenvalues of this ring-shaped waveguide structure yields multiple guided modes [the first two guided modes are shown in Figs. 5(b) and 5(c)]. In other words, the filament-induced sound wave traps the light in its crest, as is well demonstrated in Figs. 4(d)–4(h).

In conclusion, we discovered that a filament induces a transient positive index change lasting for approximately 0.5 μs, and demonstrated waveguiding through it. We also explored the formation and propagation of the sound wave resulting from the filament. This experiment demonstrates that femtosecond laser filamentation in the atmosphere leaves behind it long-lasting (microseconds) waveguiding channels. With the combination of current fiber laser technology that can drive filaments at repetition rates approaching MHz time scales [25,26], a cw laser beam can already be almost continuously guided within such a filament-induced waveguide. This ability to guide probe beams for such relatively long times offers many applications, such as, for example, power channeling of light over large distances [27]. Naturally, the ability to guide light over microseconds (instead of nanoseconds, as was the common belief thus far) improves the potential efficiency of power transmission by orders of magnitude. In a similar vein, laser filamentation can give rise to lasing [28,29]. Clearly, having waveguiding effects for extended periods of time would greatly improve applications of these lasing effects. Finally, filaments can be used for writing refractive index gratings at preselected positions in the atmosphere [30] that may be used for enhancing the stability of following filaments [31,32] and for increasing the numerical aperture of telescopes [33]. Clearly, having long-lived index changes induced by the filaments introduces many applications, which are yet to be explored.

Note added. Initially, we thought that the filament had induced a long-lived bell-shaped waveguide structure [34]. As explained above and demonstrated in Fig. 4, the filament-induced waveguide is actually annular. We acknowledge H. Milchberg for suggesting that the waveguide is annular and that it is induced by the outpropagating acoustic wave [35,36]. We also note that Milchberg's group recently demonstrated millisecond-scale waveguiding [37] by using four filaments.

This work was supported by the Technion funds for security research, which is headed by Prof. Avi Marmur, and by the Nancy and Stephen Grand Technion Energy Program (GTEP). We gratefully acknowledge the support of Prof. Mark Karpovsky of Boston University.

[1] A. Braun, G. Korn, X. Liu, D. Du, J. Squier, and G. Mourou, Opt. Lett. **20**, 73 (1995).
[2] L. Berge, S. Skupin, R. Nuter, J. Kasparian, and J.-P. Wolf, Rep. Prog. Phys. **70**, 1633 (2007).
[3] A. Couairon and A. Mysyrowicz, Phys. Rep. **441**, 47 (2007).
[4] M. Rodriguez, R. Bourayou, G. Méjean, J. Kasparian, J. Yu, E. Salmon, A. Scholz, B. Stecklum, J. Eislöffel, U. Laux, A. P. Hatzes, R. Sauerbrey, L. Wöste, and J.-P. Wolf, Phys. Rev. E **69**, 036607 (2004).
[5] J. Kasparian, M. Rodriguez, G. Méjean, J. Yu, E. Salmon, H. Wille, R. Bourayou, S. Frey, Y.-B. André, A. Mysyrowicz, R. Sauerbrey, J.-P. Wolf, and L. Wöste, Science **301**, 61 (2003).
[6] G. Méchain, A. Couairon, Y.-B. André, C. D'Amico, M. Franco, B. Prade, S. Tzortzakis, A. Mysyrowicz, and R. Sauerbrey, Appl. Phys. B **79**, 379 (2004).
[7] M. S. Mills, M. Kolesik, and D. N. Christodoulides, Opt. Lett. **38**, 25 (2013).
[8] R. Salame, N. Lascoux, E. Salmon, J. Kasparian, and J.-P. Wolf, Appl. Phys. Lett. **91**, 171106 (2007).
[9] S. L. Chin, A. Talebpour, J. Yang, S. Petit, V. P. Kandidov, O. G. Kosareva, and M. P. Tamarov, Appl. Phys. B **74**, 67 (2002).
[10] Q. Luo, H. L. Xu, S. A. Hosseini, J.-F. Daigle, F. Théberge, M. Sharifi, and S. L. Chin, Appl. Phys. B **82**, 105 (2006).
[11] P. Rohwetter *et al.*, Nat. Photonics **4**, 451 (2010).
[12] C. G. Durfee and H. M. Milchberg, Phys. Rev. Lett. **71**, 2409 (1993).
[13] C. G. Durfee, J. Lynch, and H. M. Milchberg, Phys. Rev. E **51**, 2368 (1995).
[14] S. Tzortzakis, B. Prade, M. Franco, and A. Mysyrowicz, Opt. Commun. **181**, 123 (2000).
[15] P. K. Pandey, S. L. Gupta, V. Narayanan, and R. K. Thareja, Phys. Plasmas **19**, 023502 (2012).
[16] M. Châteauneuf, S. Payeur, J. Dubois, and J.-C. Kieffer, Appl. Phys. Lett. **92**, 091104 (2008).
[17] C. D'Amico, A. Houard, M. Franco, B. Prade, A. Mysyrowicz, A. Couairon, and V. T. Tikhonchuk, Phys. Rev. Lett. **98**, 235002 (2007).
[18] B. Zhou *et al.*, Opt. Express **17**, 11450 (2009).
[19] H. Stapelfeldt and T. Seideman, Rev. Mod. Phys. **75**, 543 (2003).
[20] R. A. Bartels, T. C. Weinacht, N. Wagner, M. Baertschy, C. H. Greene, M. M. Murnane, and H. C. Kapteyn, Phys. Rev. Lett. **88**, 013903 (2001).
[21] S. Varma, Y.-H. Chen, and H. M. Milchberg, Phys. Rev. Lett. **101**, 205001 (2008).
[22] F. Calegari, C. Vozzi, and S. Stagira, Phys. Rev. A **79**, 023827 (2009).
[23] Y.-H. Cheng, J. K. Wahlstrand, N. Jhajj, and H. M. Milchberg, Opt. Express **21**, 4740 (2013).
[24] J. Yu, D. Mondelain, J. Kasparian, E. Salmon, S. Geffroy, C. Favre, V. Boutou, and J.-P. Wolf, Appl. Opt. **42**, 7117 (2003).
[25] S. Hädrich, A. Klenke, A. Hoffmann, T. Eidam, T. Gottschall, J. Rothhardt, J. Limpert, and A. Tünnermann, Opt. Lett. **38**, 3866 (2013).
[26] M. Krebs, S. Hädrich, S. Demmler, J. Rothhardt, A. Zaïr, L. Chipperfield, J. Limpert, and A. Tünnermann, Nat. Photonics **7**, 555 (2013).
[27] A. M. Rubenchik, M. P. Fedoruk, and S. K. Turitsyn, Phys. Rev. Lett. **102**, 233902 (2009).
[28] Q. Luo, W. Liu, and S. L. Chin, Appl. Phys. B **76**, 337 (2003).
[29] A. Dogariu, J. B. Michael, M. O. Scully, and R. B. Miles, Science **331**, 442 (2011).

[30] J. Liu, W. Li, H. Pan, and H. Zeng, Appl. Phys. Lett. **99**, 151105 (2011).

[31] P. Panagiotopoulos, N. K. Efremidis, D. G. Papazoglou, A. Couairon, and S. Tzortzakis, Phys. Rev. A **82**, 061803 (2010).

[32] M. Bellec, P. Panagiotopoulos, D. G. Papazoglou, N. K. Efremidis, A. Couairon, and S. Tzortzakis, Phys. Rev. Lett. **109**, 113905 (2012).

[33] E. N. Ribak, Proc. SPIE, doi:10.1117/12.802837 (2008).

[34] L. Levi, O. Lahav, R. A. Nemirovsky, J. Nemirovsky, I. Orr, I. Kaminer, M. Segev, and O. Cohen, arXiv:1307.3588.

[35] J. K. Wahlstrand, N. Jhajj, E. W. Rosenthal, S. Zahedpour, and H. M. Milchberg, Opt. Lett. **39**, 1290 (2014).

[36] E. W. Rosenthal, N. Jhajj, J. K. Wahlstrand, and H. M. Milchberg, Optica **1**, 5 (2014).

[37] N. Jhajj, E. W. Rosenthal, R. Birnbaum, J. K. Wahlstrand, and H. M. Milchberg, Phys. Rev. X **4**, 011027 (2014).